GEOSCIENCE FRONTIERS 3(5) (2012) 603–611

available at www.sciencedirect.com

China University of Geosciences (Beijing)

GEOSCIENCE FRONTIERS

journal homepage: www.elsevier.com/locate/gsf

RESEARCH PAPER

Spinel + quartz-bearing ultrahigh-temperature granulites from Xumayao, Inner Mongolia Suture Zone, North China Craton: Petrology, phase equilibria and counterclockwise *p-T* path

Huatian Zhang [a,*], Jianghai Li [a], Shoujie Liu [b], Wenshan Li [a], M. Santosh [c,d], Honghao Wang [a]

[a] *School of Earth and Space Sciences, Peking University, Beijing 100871, China*
[b] *Beijing SHRIMP Center, Institute of Geology, Chinese Academy of Geological Sciences, Beijing 100037, China*
[c] *Division of Interdisciplinary Science, Faculty of Science, Kochi University, Kochi 780-8520, Japan*
[d] *China University of Geosciences (Beijing), 29 Xueyuan Road, Beijing 100083, China*

Received 10 December 2011; received in revised form 10 January 2012; accepted 23 January 2012
Available online 11 February 2012

KEYWORDS
Ultrahigh-temperature metamorphism;
Petrology;
p-T path;
Inner Mongolia Suture Zone;
North China Craton

Abstract The Khondalite Belt within the Inner Mongolia Suture Zone (IMSZ) in the North China Craton is a classic example for Paleoproterozoic ultrahigh-temperature (UHT) metamorphism. Here we report new spinel-bearing metapelitic granulites from a new locality at Xumayao within the southern domain of the IMSZ. Petrological studies and thermodynamic modeling of the spinel + quartz-bearing assemblage shows that these rocks experienced extreme metamorphism at UHT conditions. Spinel occurs in two textural settings: 1) high X_{Zn}(Zn/(Mg + Fe^{II} + Zn) = 0.071–0.232) spinel with perthitic K-feldspar, sillimanite and quartz in the rock matrix; and 2) low X_{Zn} (0.045–0.070) spinel as inclusions within garnet porphyroblasts in association with quartz and sillimanite.

Our phase equilibria modeling indicates two main stages during the metamorphic evolution of these rocks: 1) near-isobaric cooling from 975 °C to 875 °C around 8 kbar, represented by the formation of

* Corresponding author. Tel.: +86 15120092441 (mobile).
E-mail address: htzhang@pku.edu.cn (H. Zhang).

Peer-review under responsibility of China University of Geosciences (Beijing).
doi:10.1016/j.gsf.2012.01.003

garnet porphyroblasts from spinel and quartz; and 2) cooling and decompression from 850 °C, 8 kbar to below 750 °C, 6.5 kbar, represented by the break-down of garnet. The spinel + quartz assemblage is considered to have been stable at peak metamorphism, formed through the break-down of cordierite, indicating a near isothermal compression process. Our study confirms the regional extent of UHT metamorphism within the IMSZ associated with the Paleoproterozoic subduction-collision process.

1. Introduction

Ultrahigh-temperature (UHT) granulites represent crustal metamorphism at extreme thermal conditions of $T = 900–1100$ °C and $p = 8–12$ kbar (Harley, 1998, 2004; Kelsey, 2008). UHT granulites are significant for not only evaluating the tolerance of the crust in withstanding extreme thermal conditions on a regional scale, but also in understanding the plate tectonic framework in which such extreme thermal conditions are generated (e.g., Brown, 2007; Santosh and Kusky, 2010).

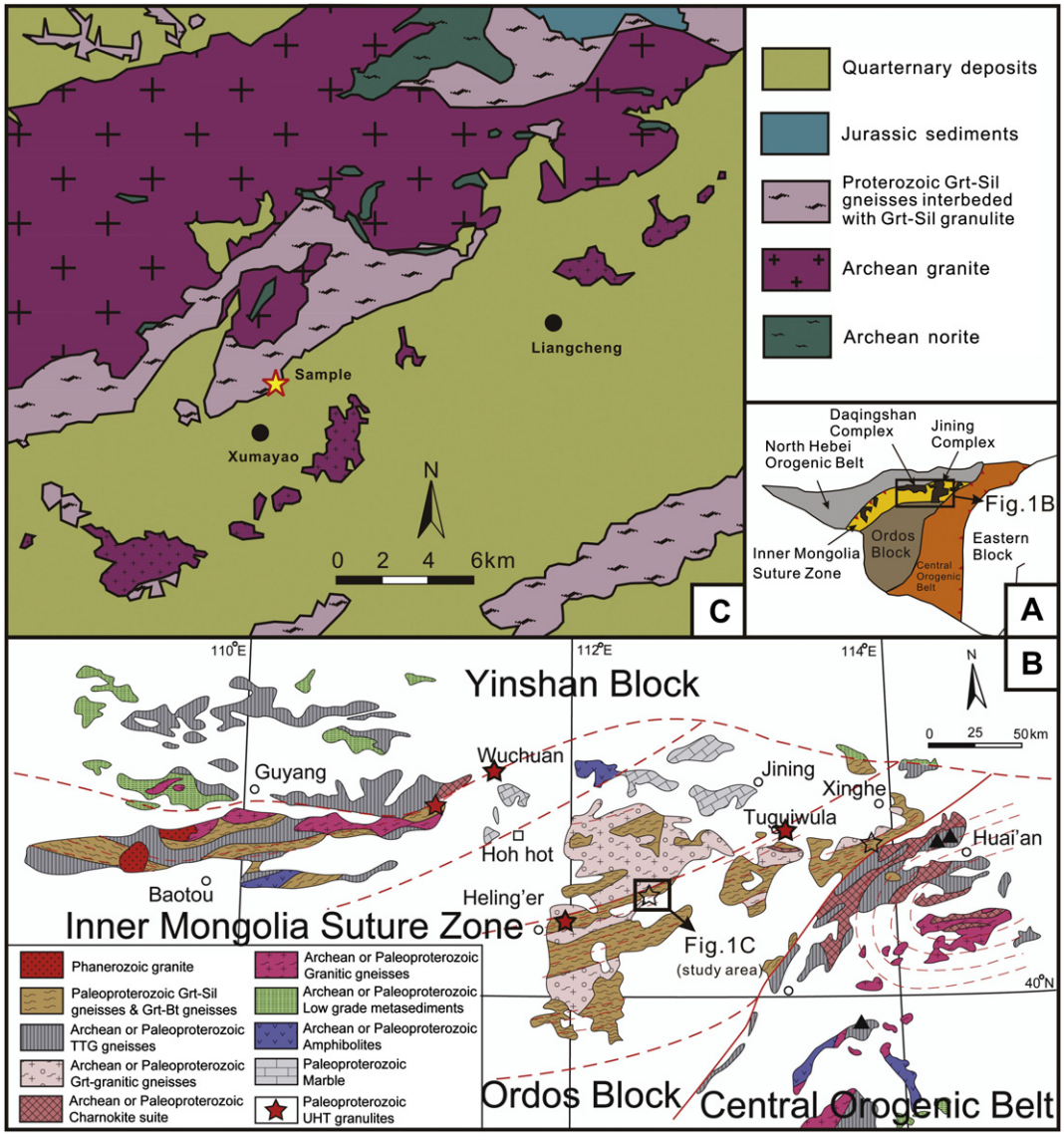

Figure 1 Geological map of North China Craton and the Inner Mongolia Suture Zone (IMSZ), with the locality of the sample discussed in this study. A: the Inner Mongolia Suture Zone marking the collisional boundary between the Yinshan and Ordos Blocks in the North China Craton (after Santosh, 2010). The study area is located in Jining Complex; B: Distribution of major lithological units within the IMSZ (after Santosh, 2010). The localities marked by red stars are the reported UHT granulites (Guo et al., 2006; Liu et al., 2008; Tsunogae et al., 2011; Santosh et al., 2006); C: Geological map of Xumayao area, Inner Mongolia. Star shows the sample location.

In the North China Craton (NCC), evidence for Paleoproterozoic UHT metamorphism was first reported from granulite facies rocks exposed within the Khondalite Belt along the northern part of the Craton by Santosh et al. (2006, 2007). Mineral assemblages diagnostic of UHT metamorphism were discovered from near Tuguiwula within the IMSZ. The Khondalite Belt in the northern part of the NCC has been the focus of several studies in the past, and has figured in critical tectonic models correlating the assembly of this craton in the Paleoproterozoic supercontinent Columbia (Zhao et al., 2002, 2005; Rogers and Santosh, 2009). Recent studies suggest that the Khondalite Belt is part of a major suture zone, termed the Inner Mongolia Suture Zone (IMSZ) developed within a subduction-accretion-collision setting (Santosh, 2010) generated during the amalgamation of the Yinshan and Ordos blocks in the NCC, the timing of which also broadly coincides with the assembly of the Paleoproterozoic supercontinent Columbia, and the incorporation of the NCC within this amalgam (Zhao et al., 2002; Rogers and Santosh, 2009). Granulite facies assemblages preserving the imprint of UHT metamorphism are now known from a number of localities from the IMSZ (Guo et al., 2006; Liu et al., 2008; Tsunogae et al., 2011; among others).

In this study, we report new spinel + quartz-bearing Mg-Al granulites from Xumayao, located toward the southern domain of the IMSZ. From petrologic studies and phase equilibria modeling, we estimate the peak *p-T* conditions to be around 950 °C and 7.8 kbar, consistent with UHT metamorphism. Our study confirms that the extreme metamorphism is of regional extent within the collisional suture.

2. Geological setting

The area investigated in this study is located in Jining Complex between Tuguiwula and Heling'er, where UHT metamorphism has been previously identified (Liu et al., 2008; Santosh, 2010). The region falls within the eastern part of IMSZ. The major rock types here are Precambrian high-grade metamorphic rocks, covered by Paleozoic and Mesozoic sedimentary rocks. Granitoid gneisses with noritic enclaves form the basement rocks including some Jurassic sandstones and shales as well as Quaternary sediments. The garnet-sillimanite gneisses (Sanggan Group) from where spinel + quartz assemblage is reported in this study occur as lenses or layers within the folded thick succession of granulite facies metapelites over the Archean basement. Santosh et al. (2006) dated the timing of ultrahigh-temperature metamorphism in this region to be 1819 ± 11 Ma (Paleoproterozoic) (Fig. 1).

3. Petrology and mineral chemistry

3.1. Petrology

The metapelitic granulites of the Xumayao region form part of the Khondalite Belt and occur as several tens of meters thick units. This Grt-Sil-Spl granulite shows prominent gneissic banding on a mm to dm scale, and exhibits obvious layering defined by garnet-rich melanocratic layers and felsic leucocratic layers (Fig. 2A).

The felsic domain is mainly composed of quartz (40%), plagioclase (28%), and perthite (20%), with minor garnet (5%), spinel (3%), biotite (2%), ilmenite (1%), and sillimanite (1%) (Figs. 2A and 3a–b). In this domain, quartz and plagioclase are medium grained (0.2–1.2 mm). Minor resorbed garnet grains are present, often associated with spinel (Fig. 3b). Spinel occurs as dark-green, subhedral minerals mostly as plagioclase inclusions (Fig. 3a). Spinel is also observed in direct contact with quartz and sillimanite (Fig. 3b). Ilmenite is fine grained, sporadically distributed among felsic minerals.

The garnet-rich part is composed of garnet (35%), sillimanite (22%), plagioclase (20%), quartz (13%), perthite (5%), spinel (3%), ilmenite (1%), and biotite (1%) (Figs. 2 and 3c–f). In this domain, garnet is coarse-grained (up to 15 mm) and porphyroblastic, and carries inclusions of fine-grained spinel, sillimanite, ilmenite and quartz (Figs. 2B and 3c–f). The garnet commonly shows exsolution texture with thin lamellae of rutile. Plagioclase and quartz are medium grained (0.2–1.2 mm), filling the matrix of garnet and sillimanite (Fig. 3c–f). Spinel is found as fine-grained inclusions (0.1–1 mm) in garnet in association with quartz within the same garnet grain, although they are not in direct contact (Fig. 3c–f). The spinel inclusions are also

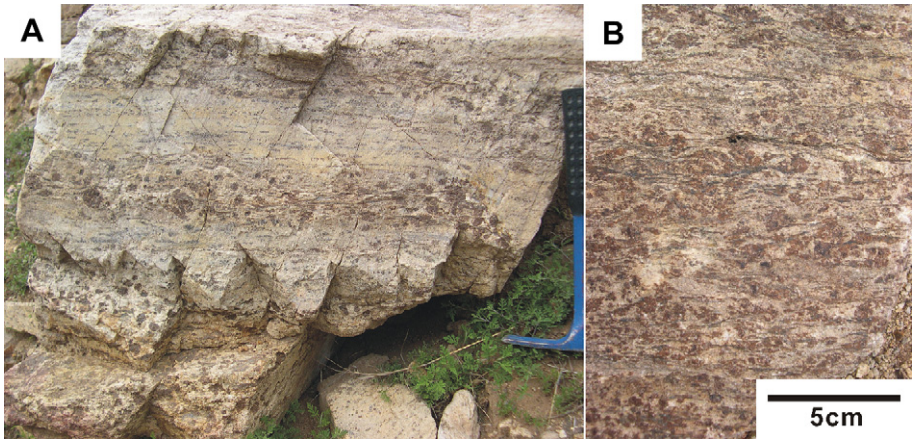

Figure 2 Field photographs of the spinel + quartz-bearing ultrahigh-temperature granulites at Xumayao in the North China Craton. A: Interbedded garnet-rich layers and felsic layers. B: Garnet-rich domain in the UHT granulites with coarse-grained garnet porphyroblasts surrounded by plagioclase and spinels as garnet inclusions.

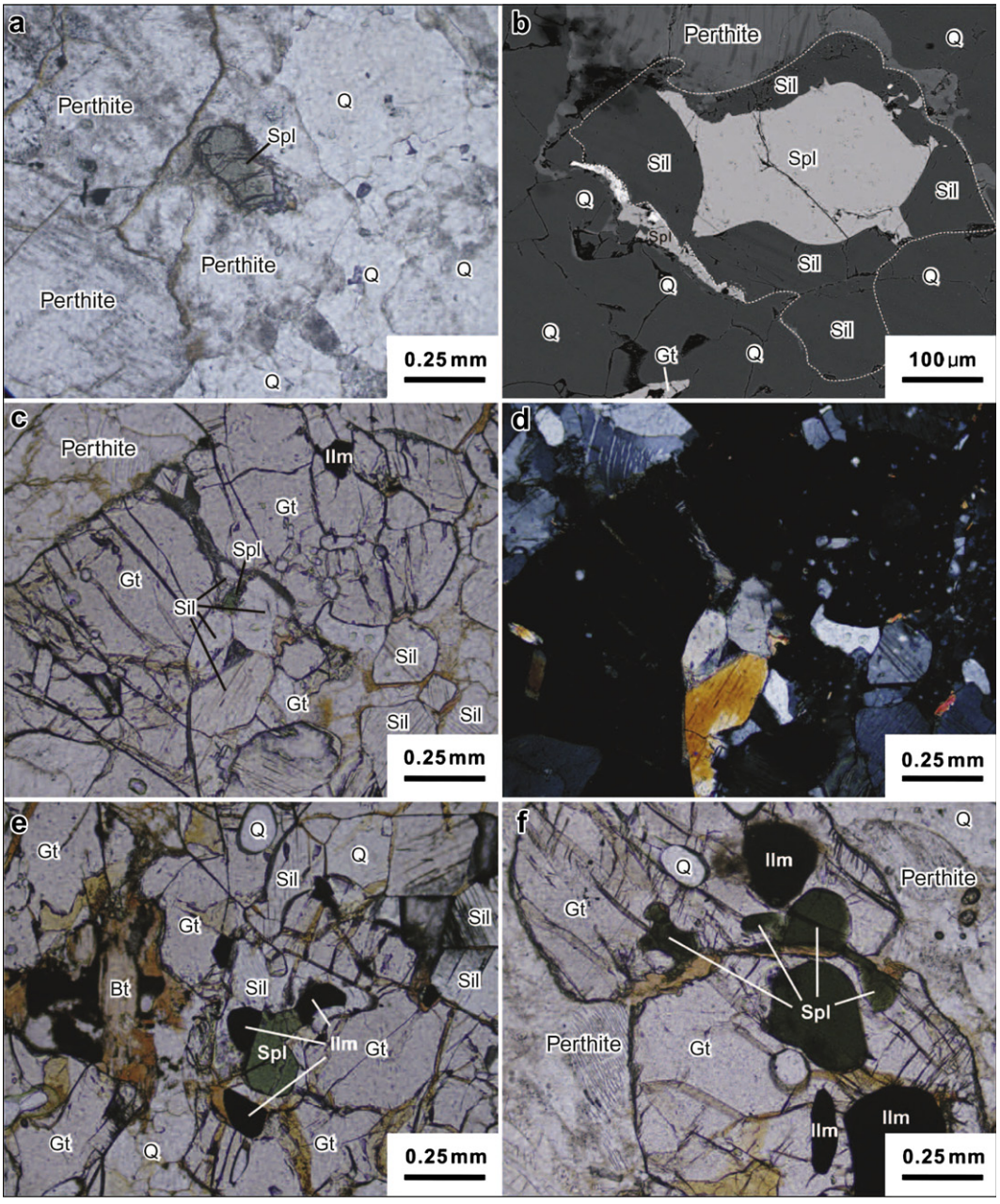

Figure 3 Photomicrographs of representative Spinel + quartz-bearing granulites discussed in this study. a: Matrix spinel in association with perthite. b: BSE image of spinel in direct contact with sillimanite and quartz. c–f: Spinel occurring as inclusions of garnet porphyroblast in association with quartz and sillimanite. Xenomorphic biotites occur along broken margins of porphyroblastic garnets.

typically associated with sillimanite (Fig. 3c–e). Sillimanite is subidioblastic and occur as inclusions in garnet associated with quartz, spinel, and ilmenite (Fig. 3c and e). Fine-grained ilmenite occurs as inclusion in garnet porphyroblasts, in association with spinel (Fig. 3c–f). Retrograde biotite is xenomorphic along the fractured garnet grains (Fig. 3e and f).

The inclusion assemblage of Spl + Qtz, with typical association with sillimanite, all included within garnet porphyroblasts (Fig. 3c–f) is of particular interest. The Grt + Sil assemblage is inferred to be peak assemblage. The two assemblages can be related by the reaction Spl + Qtz = Grt + Sil. Although the reaction Sil + Grt = Spl + Qtz would produce spinel and quartz, the resulting texture should display spinel and quartz in direct contact with the consumption of either garnet or sillimanite, a texture which is not observed in our samples. Therefore we prefer the following reaction to represent the peak metamorphic reaction (the growth of garnet) (Fig. 4b):

$$\mathrm{Spl} + \mathrm{Qtz} = \mathrm{Grt} + \mathrm{Sil} \quad (1)$$

The occurrence of secondary biotite (Fig. 3e and f) is inferred to be retrograde assemblage, formed by the following reaction:

$$\mathrm{Grt} + \mathrm{H_2O} = \mathrm{Bt} + \mathrm{Sil} + \mathrm{Qtz} \quad (2)$$

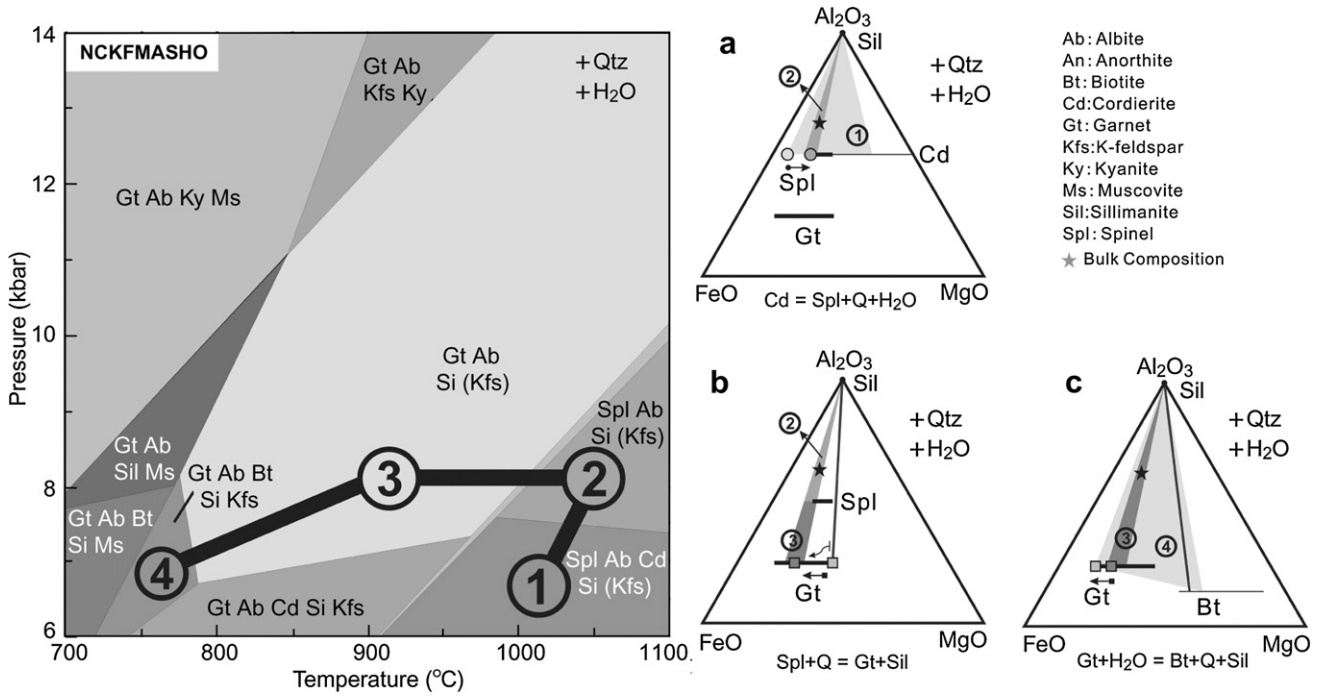

Figure 4 Simplified *p-T* projection (Kfs-absent univariant line is overlooked) showing the four stable mineral assemblages, and Al_2O_3-FeO-MgO diagram with saturated SiO_2 and water. The four stable assemblages are: ①Ab + Crd + Sil ± Grt/Spl ± Kfs; ②Spl + Ab + Sil ± Kfs; ③Grt + Ab + Sil ± Kfs; ④Grt + Ab + Bt + Sil + Kfs. Thick lines of spinel and garnet represent the actual mineral compositions analyzed by electron microprobe. See text for detailed discussion.

3.2. Mineral chemistry

Representative mineral compositions were obtained through Electron Microprobe Analysis on thin sections from a representative sample collected from Xumayao area (Fig. 1C). The EPMA analysis was performed using a JXA-8100 microprobe housed at the Peking University, with instrument conditions of 15 kV accelerating voltage and 10 nA sample current. The data were regressed using a PRZ correction. Fe^{3+} was calculated based on stoichiometry. Representative analytical data are given in Table 1 and the mineral compositions are briefly discussed below.

3.2.1. Garnet

Porphyroblastic garnet in garnet-rich domain is essentially a solid solution of almandine and pyrope ($Alm_{49-57}Pyr_{38-43}And_{2-9}Sps_{0-1}$ for most porphyroblastic garnets analyzed). They display a slight rimward decrease of X_{Mg} from 0.41−0.45 to 0.40−0.44, and obvious increase of X_{Ca} from 0.0200−0.0259 to 0.0250−0.0264 (Tables 1 and 3), where XMgnbsp=nbspMg/(Mgnbsp+nbspFe) and XCanbsp=nbspCa/(Canbsp+nbspMgnbsp+nbspFe)

3.2.2. Spinel

Spinel is mostly Al-series spinel, with a typical average $Al:Fe^{III}:Cr = 97.9:0.3:1.8$. The Al-series spinel is essentially a solid solution of hercynite and Mg-spinel, together with Zn-spinel component. The composition of spinel varies depending on its occurrence. The spinels in the matrix show lower Mg and much higher Zn component as compared with those occurring as inclusions in garnets ($X_{Mg} = Mg/(Mg + Fe) = 0.27-0.38$ and $X_{Zn} = Zn/(Mg + Fe + Zn) = 0.064-0.232$ for spinels in matrix; $X_{Mg} = 0.32-0.42$ and $X_{Zn} = 0.048-0.073$ for spinels occurring as inclusions in garnet). The spinel grains generally display a rimward increase of X_{Mg} (Tables 1 and 3).

3.2.3. Other minerals

Plagioclase in these rocks is a matrix mineral and shows a composition of $An_{0.25-0.27}Ab_{0.73-0.75}$. Biotite is xenomorphic with annite and phlogopite components ($Ann_{0.17}Phl_{0.83}$). Sillimanite is close to the ideal chemistry of Al_2SiO_5, although it contains small amounts of Fe^{3+} and Cr (Al: Fe^{3+}: Cr = 1.976:0.013:0.003). Ilmenite contains minor Mg and Mn (Fe^{2+}: Mg: Mn = 0.911:0.087:0.002).

4. Mineral phase equilibria modeling

Mineral phase equilibria calculations were carried out by THERIAK-DOMINO (Version 01.08.09) by De Capitani and Brown (1987) in the system Na_2O-CaO-K_2O-FeO-MgO-Al_2O_3-SiO_2-H_2O-Fe_2O_3 (NCKFMASHO). The bulk compositions were estimated based on mode (Vol%), density (Holland and Powell, 1998) and analyzed compositions of minerals (Table 2), and as described by Wei et al. (2003). The resultant bulk composition is listed in Table 2. Minor minerals including zircon and rutile are not taken into the calculation. Oxygen content is estimated through positive ions contents (Fe^{3+} included) by means of stoichiometry, so that the oxidization/reduction condition can be taken into consideration. In addition, excess H_2O content is assumed for the calculation. The validity of this assumption will be discussed in the following paragraph. The calculated pseudosection is shown in Fig. 5.

Table 1 Representative electron microprobe analyses of major minerals in the sample. Compositions of two typical garnets, five spinels in different environments, as well as one perthite, plagioclase, sillimanite, biotite and ilmenite, are listed. X_{Mg} = Mg/(Mg + Fe), X_{Ca} = Ca/(Ca + Mg + Fe), X_{Zn} = Zn/(Zn + Mg + Fe).

Mineral	Garnet-1		Garnet-2		Spinel									Perthite		Pl	Sil	Bt	Ilm
Remarks	+spl + qtz		+spl − qtz		As inclusion (−qtz)		As inclusion (+qtz)		Matrix (+pl)		Matrix (+sil)		Matrix (+qtz)	Pl	Kfs	−	−	−	−
	Core	Rim	Core	Rim	Core	Rim	Core	Rim	Core	Rim	Core	Rim		−	−	−	−	−	−
No.	2−39	2−41	2−15	2−16	2−43	2−44	2−17	2−18	2−81	2−82	3−1	3−2	3−6	−	−	−	−	−	−
SiO_2	39.37	39.38	39.40	39.61	0.05	0.77	0.08	0.11	0.10	0.01	0.04	0.03	0.31	60.03	64.24	61.01	37.08	38.57	0.03
TiO_2	0.04	0.00	0.00	0.06	0.09	0.04	0.02	0.05	0.00	0.00	0.05	0.00	0.04	0.05	0.06	0.03	0.02	4.62	53.62
Al_2O_3	21.65	21.88	21.68	22.20	60.84	60.03	59.26	59.71	59.42	58.74	58.30	58.20	60.25	24.02	18.34	23.95	61.52	13.38	0.06
Cr_2O_3	0.01	0.03	0.04	0.07	1.20	1.31	2.14	2.05	1.63	1.64	2.51	2.46	2.26	0.00	0.03	0.02	0.16	0.09	0.15
FeO	26.96	27.15	27.90	27.58	21.90	20.81	24.81	24.92	22.08	22.01	22.22	22.03	20.93	0.03	0.00	0.03	0.64	7.94	44.85
MnO	0.28	0.28	0.17	0.24	0.00	0.07	0.04	0.04	0.06	0.09	0.03	0.00	0.03	0.00	0.00	0.03	0.03	0.03	0.06
MgO	11.22	10.84	10.47	10.55	11.58	11.7	10.79	11.11	8.83	8.69	9.22	9.53	9.84	0.02	0.00	0.00	0.00	19.14	2.31
CaO	0.95	0.96	0.87	0.92	0.00	0.07	0.02	0.00	0.04	0.00	0.00	0.00	0.00	5.93	0.10	5.38	0.02	0.07	0.02
ZnO	0.00	0.00	0.00	0.03	4.88	4.36	3.37	3.28	7.57	7.41	6.17	6.39	6.79	0.03	0.00	0.00	0.10	0.00	0.06
Na_2O	0.02	0.11	0.12	0.03	0.08	0.28	0.12	0.11	0.24	0.24	0.28	0.21	0.21	8.37	1.23	8.92	0.02	0.24	0.10
K_2O	0.03	0.00	0.01	0.00	0.00	0.03	0.00	0.00	0.00	0.00	0.01	0.00	0.00	0.24	15.05	0.16	0.01	10.24	0.05
Total	100.55	100.7	100.66	101.31	100.73	99.57	100.74	101.47	100.24	99.04	98.96	99.01	100.86	98.74	99.13	99.56	99.63	94.38	101.32
Oxygen	12	12	12	12	4	4	4	4	4	4	4	4	4	8	8	8	5	11	3
Si	2.984	2.983	2.995	2.991	0.001	0.022	0.002	0.003	0.000	0.003	0.001	0.001	0.009	2.695	2.980	2.709	1.007	2.891	0.001
Ti	0.002	0.000	0.000	0.003	0.002	0.001	0.000	0.001	0.000	0.000	0.001	0.000	0.001	0.002	0.000	0.001	0.000	0.260	0.988
Al	1.934	1.954	1.942	1.975	2.005	1.993	1.963	1.962	1.990	1.988	1.974	1.971	2.000	1.271	1.000	1.253	1.969	1.182	0.001
Cr	0.001	0.002	0.002	0.004	0.027	0.029	0.048	0.045	0.037	0.037	0.057	0.056	0.05	0.000	0.000	0.001	0.003	0.005	0.001
Fe_T	1.709	1.720	1.774	1.742	0.512	0.49	0.583	0.581	0.529	0.524	0.534	0.529	0.492	0.001	0.000	0.001	0.015	0.498	0.919
Mn	0.018	0.018	0.011	0.015	0.000	0.002	0.001	0.001	0.002	0.001	0.001	0.000	0.001	0.000	0.000	0.001	0.001	0.002	0.001
Mg	1.268	1.224	1.186	1.187	0.346	0.352	0.324	0.331	0.267	0.268	0.283	0.292	0.295	0.001	0.000	0.000	0.000	2.139	0.084
Ca	0.078	0.078	0.071	0.074	0.000	0.002	0.001	0.000	0.000	0.001	0.000	0.000	0.000	0.285	0.000	0.256	0.001	0.006	0.001
Zn	0.000	0.003	0.000	0.002	0.101	0.091	0.070	0.068	0.157	0.159	0.131	0.136	0.141	0.001	0.000	0.000	0.002	0.000	0.001
Na	0.003	0.016	0.004	0.001	0.004	0.015	0.007	0.006	0.013	0.013	0.016	0.012	0.011	0.729	0.110	0.768	0.001	0.035	0.002
K	0.003	0.000	0.000	0.000	0.000	0.001	0.000	0.000	0.000	0.000	0.000	0.000	0.000	0.014	0.890	0.009	0.000	0.979	0.001
Total	8.000	7.998	7.985	7.994	2.998	2.998	2.999	2.998	2.995	2.994	2.998	2.997	3.000	4.999	4.997	4.999	2.999	7.996	2.000
Fe_{III}	0.098	0.094	0.084	0.036	0.000	0.000	0.000	0.000	0.000	0.000	0.000	0.000	0.000	−	−	−	−	0.045	0.024
Fe_{II}	1.611	1.626	1.689	1.705	0.512	0.49	0.583	0.581	0.529	0.524	0.534	0.529	0.492	−	−	−	−	0.453	0.895
Alm	0.529	0.540	0.560	0.574	−	−	−	−	−	−	−	−	−	−	−	−	−	−	−
Pyr	0.416	0.406	0.393	0.400	−	−	−	−	−	−	−	−	−	−	−	−	−	−	−
And	0.049	0.047	0.042	0.018	−	−	−	−	−	−	−	−	−	−	−	−	−	−	−
X_{Mg}	0.440	0.429	0.413	0.410	0.403	0.418	0.357	0.363	0.335	0.338	0.346	0.356	0.375	−	−	−	−	−	−
X_{Ca}	0.0259	0.0265	0.0240	0.0250	−	−	−	−	−	−	−	−	−	−	−	−	−	−	−
X_{Zn}	−	−	−	−	0.105	0.097	0.072	0.069	0.165	0.167	0.138	0.142	0.152	−	−	−	−	−	−

Table 2 Bulk composition used for mineral phase equilibria calculation. It is estimated based on mode (Vol%), density (Holland and Powell, 1998) and analyzed compositions of minerals, as described by Wei et al. (2003). Oxygen is estimated through positive ions (Fe^{3+} and H included). Water is assumed to be in access.

Compositional domains	Mineral assemblage and average bulk composition
Felsic domain	Qtz(40%) + Pl(28%) + Perthite(20%) + Grt(5%) + Spl(3%) + Bt(2%) + Ilm(1%) + Sil(1%)
Garnet-rich domain	Grt(35%) + Sil(22%) + Pl(20%) + Qtz(13%) + Perthite(5%) + Spl(3%) + Ilm(1%) + Bt(1%)
Bulk composition	Bulk = felsic domain (55%) + garnet-rich domain (45%) = Si(44.02)Al(37.34)Fe(7.91)Mg(3.01)Ca(1.23)Na(3.34)K(1.73)H(60)O(188.96)

The H_2O component has significant effect on the location of mineral equilibria in FMAS(H) (Kelsey et al., 2004). It is generally evaluated by distinguishing the stability of minerals on $T - M_{H_2O}$ pseudosection at a defined pressure (see for example, Tsunogae et al., 2011) or the solidus on $T - X_{H_2O}$ pseudosection as described by White et al. (2001) (see for example, Dharma Rao et al., 2012), in order that it is approximately at the point where the equilibrium assemblage was sufficiently saturated. In this study, however, the H_2O content is assumed to be in excess (H_2O exists as stable phase in all the divariant domains examined). In order to figure out the possible effects of H_2O on the locations of stable assemblages, we made several *p-T* grids with various H_2O content. The results show that apart from the completely anhydrous condition ($H_2O = 0$), in all the other *p-T* grids, there is undetectable difference except for the H_2O-absent univariant lines. The H_2O-absent univariant line moves toward lower pressure and temperature with increasing H_2O content. The observation that secondary biotite formed during retrograde metamorphism confirms the presence of water in the system. We therefore assume an excess H_2O content in the equilibria modeling.

According to the metamorphic textures observed and discussion above, the metapelitic granulite sample has undergone two major reactions: 1) the transformation from spinel + quartz to garnet (Fig. 3c–f), and 2) the break-down of garnet to form biotite (Fig. 3e and f). These two reactions are clearly recorded in our samples and are depicted in the *p-T* diagram shown in Fig. 4, where the two stages are denoted by the thick line linking encircled number 2, 3 and 3, 4 separately.

These two stages are illustrated on Al_2O_3-FeO-MgO diagram to show the changes of mineral compositions (Fig. 4b and c). Thermodynamic calculation suggests that the reaction from spinel to garnet and sillimanite consumes more Mg-spinel compared to the overall X_{Mg} of spinel. Therefore, the spinels with more hercynite are retained, which is presented by the thick Spl-line (Fig. 4b). Meanwhile garnet is formed, with a rimward decrease of X_{Mg} (shown by rectangular in Fig. 4b). The equilibrium assemblages change from Spl + Sil to Grt + Sil. On producing garnet porphyroblast, spinel and quartz are separated, thus terminating the reaction between them. In the second stage, garnet breaks down to biotite by consuming more pyrope than almandine, drawing garnet to move further toward Fe-component (shown by rectangular in Fig. 4c). The equilibrium assemblages change from Grt + Sil to Grt + Bt + Sil.

The stability of spinel + quartz (with cordierite) moves toward lower temperature and higher pressure with the increase of Zn component (Nichols et al., 1992). This is shown in Fig. 5 by red dashed lines, which denotes for the spinel + quartz stability from higher to lower temperature. Therefore, if the reaction Spl + Qtz = Grt + Sil occurs, the spinel + quartz (with the Zn component taken into consideration) equilibrium must be the same with that of the initial formation of garnet, which can be characterized by the components of garnet in direct contact with spinel. This means that the intersection of X_{Zn} line of spinel (red dashed line in Fig. 5) with X_{Ca} line of garnet (black solid line in Fig. 5) represents the transformation of the *p-T* stability from spinel to garnet.

The X_{Zn} value of spinels both in matrix and those occurring as inclusions within porphyroblastic garnets (Table 3), define a domain in Fig. 5 (shown by white rectangle) which represents the *p-T* condition of the reaction Spl + Qtz = Grt + Sil.

Subsequently, the garnets continued to grow until spinel and quartz were completely separated, thus inhibiting their reactions and forming the texture of isolated spinel and quartz grains occurring as islands within porphyroblastic garnet in association with sillimanite as observed in the sample (Fig. 3c–f). The highest X_{Ca} value (0.0266) among all the garnet gains analyzed suggests that the *p-T* path passed through $X_{Ca} \approx 0.027$ in Fig. 5 (indicated by black solid line).

The break-down of garnet into biotite defines another (retrograde) *p-T* domain within the biotite stable field, indicating a cooling process. The *p-T* path is constrained in the field where muscovite and cordierite are unstable (Fig. 5), as these minerals do not occur in the sample.

The two *p-T* domains discussed above define the peak and retrograde metamorphic conditions as shown in Fig. 5 with black solid arrow. Here we further address the possible formation process of spinel and quartz. Because the position of Mg isolines of spinel cannot be precisely defined in the *p-T* diagram with variable Zn content, the actual *p-T* conditions of formation of spinel + quartz is difficult to estimate. However, it is apparent

Table 3 Representative garnet and spinel analysis used for *p-T* phase equilibria modeling.

Mineral	Garnet										Spinel					
Remarks	Core → Rim				Core → Rim			Core → Rim			Core	Rim	Core	Rim	Core	Rim
No.	2–27	2–28	2–29	2–30	2–40	2–41	2–42	2–46	2–47	2–48	2–25	2–26	2–43	2–44	2–17	2–18
X_{Ca}	0.0228	0.0242	0.0247	0.0255	0.0247	0.0264	0.0264	0.0239	0.0245	0.0253	–	–	–	–	–	–
X_{Zn}	–	–	–	–	–	–	–	–	–	–	0.055	0.052	0.072	0.069	0.051	0.054

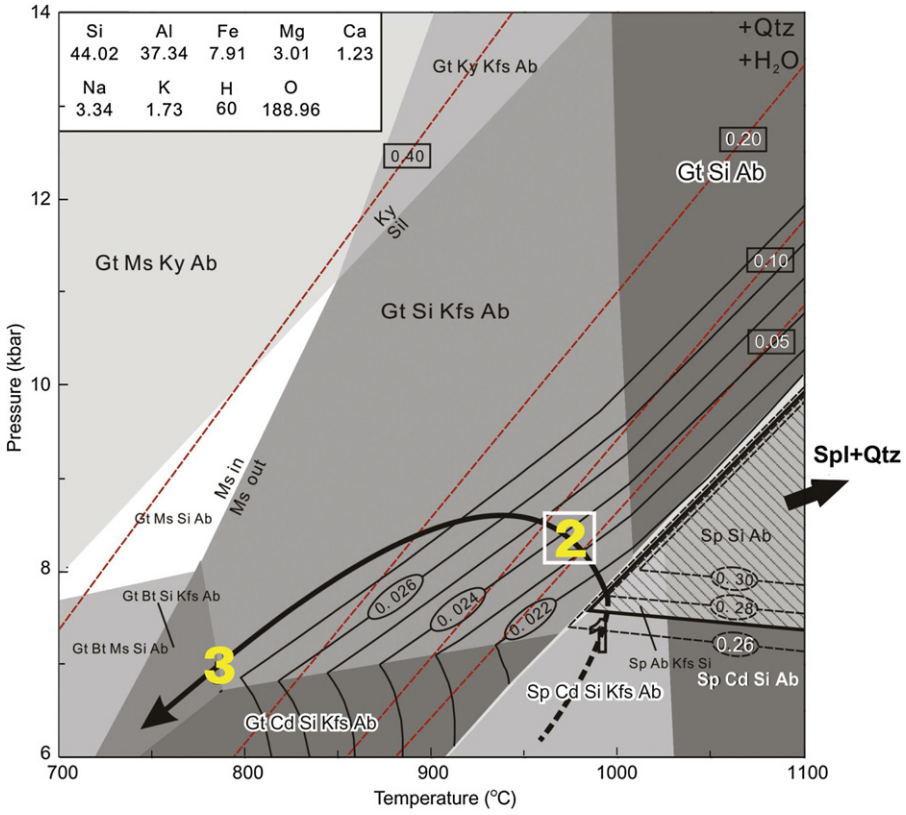

Figure 5 Calculated *p-T* pseudosection for the sample. Calculations were undertaken in the system Na_2O-CaO-K_2O-FeO-MgO-Al_2O_3-SiO_2-H_2O-Fe_2O_3 (NCKFMASHO), using THERIAK-DOMINO (Version 01.08.09) by De Capitani and Brown (1987). The arrow stands for the *p-T* path of the sample inferred in this study. The *p-T* path is divided into three major steps, annotated by hollowed numbers 1–3 respectively, among which the first step is represented by dashed line, implying that this step is not sufficiently verified. Solid lines with numbers encircled by eclipses represent X_{Ca} isopleth of garnet. Dashed lines with numbers encircled by dashed eclipses represent X_{Mg} isopleth of spinels. Both isopleths are calculated under the Zn-free NCKFMASHO system. However, when Zn component of spinel is taken into consideration, the stability area of spinel + quartz moves toward lower temperature and higher pressure, which is represented by red lines with X_{Zn} values framed by rectangulars. White rectangular represents the transformation of the *p-T* stability from spinel to garnet.

from the *p-T* pseudosection that with the increase in pressure or temperature, the X_{Mg} value of spinels also increases (Fig. 5). This can be illustrated on the Al_2O_3-FeO-MgO diagram. On crossing the univariant reaction:

$$Crd = Spl + Qtz + H_2O \quad (3)$$

spinel is formed with a rimward increase of Mg-spinel component (shown in Fig. 4a by thick solid line and arrow). The stable assemblages change from Spl + Crd + Sil to Spl + Sil (Fig. 4a). Therefore, the rise of Mg component of the spinels in this rock (Tables 1 and 3) suggests compression or heating process, which produced the peak mineral assemblage of spinel + quartz. Between the two processes, compression is more preferred. The reason is as follows: a heating process that breaks garnets to form spinel + quartz will generate anorthite at the same time, which means feldspars would probably be found as inclusions in garnet porphyroblasts. However, no such texture is found in the sample, indicating an alternative process of compression that produces spinel + quartz without anorthite. Therefore, the Mg compositional zoning provides a robust indication of the near isothermal compression process accompanying the reaction (Fig. 4a). Unfortunately, no direct evidence for the resulting texture is seen in these rocks and therefore the above inference remains tentative.

The three reactions discussed above outline a counterclockwise *p-T* path in the *p-T* pseudosection (Fig. 5):

1) (possible) near isothermal compression to 7.3 kbar around 975 °C, represented by the break-down of cordierite into spinel and quartz;
2) near-isobaric cooling from 975 °C to 875 °C around 8 kbar, represented by the formation of garnet porphyroblasts from spinel and quartz;
3) cooling and decompression process from 850 °C, 8 kbar to below 750 °C, 6.5 kbar, represented by the break-down of garnet into biotite.

5. Summary and conclusion

The petrographic and microstructural studies, combined with mineral phase equilibria modeling of spinel-bearing metapelitic granulites from a new locality at Xumayao in the Khondalite Belt in the North China Craton reveal a counterclockwise *p-T* path involving three major steps: 1) (possible) near isothermal compression to 7.3 kbar around 975 °C, represented by the break-down of cordierite into spinel and quartz; 2) near-isobaric cooling

from 975 °C to 875 °C around 8 kbar, represented by the formation of garnet porphyroblasts from spinel and quartz; and 3) cooling and decompression process from 850 °C, 8 kbar to below 750 °C, 6.5 kbar, represented by the break-down of garnet into biotite. Our study defines the stability of spinel + quartz assemblage in these rocks as $T > 950$ °C and $p > 7.5$ kbar, consistent with UHT metamorphic conditions. Our results closely compare with the *p-T* estimates reported in previous studies from sapphirine-bearing UHT granulites in different localities within the IMSZ using various mineral thermobarometers and pseudosection computations (reviewed in Santosh et al., in press). The finding of UHT rocks in Xumayao indicates that the extreme crustal metamorphism is of regional extent within the northern margin of the North China Craton.

Acknowledgments

We thank Prof. T. Tsunogae for field discussion and helpful suggestions in revising the manuscript. We also thank Dr. C.V. Dharma Rao for valuable comments on the earlier version of this manuscript. Special thanks to Prof. S.G. Song, Peking University, for his guidance in processing data. We are also grateful to Mr. G.M. Shu, technical staff from Peking University, for his assistance on microprobe analysis.

References

Brown, M., 2007. Metamorphic conditions in orogenic belts: a record of secular change. International Geology Review 49, 193−234.

De Capitani, C., Brown, T.H., 1987. The computation of chemical equilibrium in complex systems containing non-ideal solutions. Geochimica et Cosmochimica Acta 51 (10), 2639−2652.

Dharma Rao, C.V., Santosh, M., Chmielowski, R.M., 2012. Sapphirine granulites from Panasapattu, Eastern Ghats belt, India: ultrahigh-temperature metamorphism in a Proterozoic convergent plate margin. Geoscience Frontiers 3 (1), 9−31.

Guo, J.H., Chen, Y., Peng, P., Liu, F., Cheng, L., Zhang, L.Q., 2006. Sapphirine bearing granulite in Daqingshan, Inner Mongolia: 1.8 Ga UHT metamorphic event. Abstract Volume of Petrology and Earth Dynamics in China.

Harley, S.L., 1998. On the occurrence and characterization of ultrahigh-temperature crustal metamorphism. In: Treloar, P.J., O'Brien, P.J. (Eds.), What Drives Metamorphism and Metamorphic Relations? Special Publications. Geological Society, London, pp. 81−107.

Harley, S.L., 2004. Extending our understanding of ultrahigh temperature crustal metamorphism. Journal of Mineralogical and Petrological Sciences 99, 140−158.

Holland, T.J.B., Powell, R., 1998. An internally consistent thermodynamic data set for phases of petrological interest. Journal of Metamorphic Geology 16 (3), 309−343.

Kelsey, D.E., White, R.W., Holland, T.J.B., Powell, R., 2004. Calculated phase equilibria in K_2O-FeO-MgO-Al_2O_3-SiO_2-H_2O for sapphirine-quartz-bearing mineral assemblages. Journal of Metamorphic Geology 22, 559−578.

Kelsey, D.E., 2008. On ultrahigh-temperature crustal metamorphism. Gondwana Research 13 (1), 1−29.

Liu, S.J., Li, J.H., Santosh, M., 2008. Ultrahigh temperature metamorphism of Tuguiwula Khondalite belt, Inner Mongolia: metamorphic reaction texture and P−T indication. Acta Petrologica Sinica 24 (6), 1185−1192 (in Chinese with English abstract).

Nichols, G.T., Berry, R.F., Green, D.H., 1992. Internally consistent gahnitic spinel-cordierite-garnet equilibira in the FMASHZn system: geothermobarometry and application. Contributions to Mineralogy and Petrology 111 (3), 362−377.

Rogers, J.J.W., Santosh, M., 2009. Tectonics and surface effects of the supercontinent Columbia. Gondwana Research 15 (3−4), 373−380.

Santosh, M., 2010. Assembling North China Craton within the Columbia supercontinent: the role of double-sided subduction. Precambrian Research 178 (1−4), 149−167.

Santosh, M., Kusky, T., 2010. Origin of paired high pressure−ultrahigh-temperature orogens: a ridge subduction and slab window model. Terra Nova 22 (1), 35−42.

Santosh, M., Liu, S.J., Tsunogae, T., Li, J.H. Paleoproterozoic ultrahigh-temperature granulites in the North China Craton: implications for tectonic models on extreme crustal metamorphism. Precambrian Research, in press.

Santosh, M., Tsunogae, T., Li, J.H., Liu, S.J., 2007. Discovery of sapphirine-bearing Mg−Al granulites in the North China Craton: implications for Palaeoproterozoic ultrahigh temperature metamorphism. Gondwana Research 11 (3), 263−285.

Santosh, M., Sajeev, K., Li, J.H., 2006. Extreme crustal metamorphism during Columbia supercontinent assembly: evidence from North China Craton. Gondwana Research 10 (3−4), 256−266.

Tsunogae, T., Liu, S.J., Santosh, M., Shimizu, H., Li, J.H., 2011. Ultrahigh-temperature metamorphism in Daqingshan, Inner Mongolia Suture Zone, North China Craton. Gondwana Research 20 (1), 36−47.

Wei, C.J., Powell, R., Zhang, L.F., 2003. Calculated mineral equilibria for eclogites from the south Tianshan, NW China. Journal of Metamorphic Geology 21, 163−180.

White, R.W., Powell, R., Holland, T.J.B., 2001. Calculation of partial melting equilibria in the system Na_2O-CaO-K_2O-FeO-MgO-Al_2O_3-SiO_2-H_2O (NCKMASH). Journal of Metamorphic Geology 19, 139−153.

Zhao, G.C., Cawood, P.A., Wilde, S.A., Sun, M., 2002. Review of global 2.1−1.8 Ga collisional orogens and accreted cratons: a pre-Rodinia supercontinent? Earth Science Review 59, 125−162.

Zhao, G., Sun, M., Wilde, S.A., Li, S., 2005. Late Archean to Paleoproterozoic evolution of the North China Craton: key issues revisited. Precambrian Research 136, 177−202.